Advanced Optical Materials

ADVANCED OPTICAL MATERIALS
www.advopticalmat.de

RESEARCH ARTICLE OPEN ACCESS

Gain Narrowing in Low-Dimensional PEA:$CsPbBr_3$: Superfluorescence versus Amplified Spontaneous Emission

Pirmin Tischler[1] | Valerie Y. Horter[1] | Yang Li[2] | Holger Geßwein[3] | Weimu Xu[1] | Renjun Guo[1,4] | Orlando Torres Perales[1] | Julian Petry[1,4] | Ulrich W. Paetzold[1,4] | Nils W. Rosemann[1] | Uli Lemmer[1,4]

[1]Light Technology Institute, Karlsruhe Institute of Technology (KIT), Karlsruhe, Germany | [2]College of Materials Science and Engineering & Engineering Research, Center of Alternative Energy Materials and Devices, Ministry of Education, Sichuan University, Chengdu, China | [3]Institute For Applied Materials, Karlsruhe Institute of Technology (KIT), Eggenstein-Leopoldshafen, Germany | [4]Institute of Microstructure Technology, Karlsruhe Institute of Technology (KIT), Eggenstein-Leopoldshafen, Germany

Correspondence: Pirmin Tischler (pirmin.tischler@kit.edu)

Received: 4 March 2026 | **Revised:** 30 June 2026 | **Accepted:** 30 July 2026

Keywords: amplified spontaneous emission | lasing | perovskite | superfluorescence | waveguides

ABSTRACT

Quantum phenomena typically occur for low temperatures. Moreover, single-molecule and single-particle spectroscopy have revealed a plethora of quantum phenomena in photonics. Superfluorescence (SF) is a macroscopic quantum effect where a macroscopic ensemble of emitters become coherent above a certain excitation threshold and cooperatively emit a burst of coherent photons. Amplified spontaneous emission (ASE), on the other hand, is a collective emission process where a spontaneously emitted photon propagates inside the emitter material and induces stimulated emission. Both SF and ASE lead to a narrow peak rising out of the photoluminescence spectrum. Recently, SF at room temperature was invoked for the explanation of spectral narrowing in low-dimensional PEA:$CsPbBr_3$ under high excitation. Here, we investigate the emission characteristics of this material and clarify whether ASE or SF is responsible for the emission narrowing. We do so by testing the effect on samples processed on different substrates, thereby manipulating the optical waveguide characteristics of the stack. We show, that the narrow emission peak is suppressed for substrates with a refractive index higher than the active material. This results from the absence of waveguide modes. These findings show that ASE—not SF—is the dominant mechanism responsible for the observed spectral narrowing.

1 | Introduction

Quantum phenomena arise due to quantized energy levels, discrete states, coherence and/or wavefunction interactions. Since these depend on properties of particles and are typically less pronounced at high temperatures due to discrete quantum states blurring into a continuum and temperature sensitive coherence times, most quantum effects can only be observed for low temperatures. Identifying observable quantum effects on a macroscopic scale at room temperature is subject of intense research as it promises a major simplification of quantum information technologies [1–3]. Superfluorescence (SF) at room temperature is regarded as a promising approach in this respect. Macroscopic coherence is an integral part of the effect of SF. Given a sufficient density of excited states in a material, a large number of these excited states cooperatively form a macroscopic coherent quantum state with a single wave function that spontaneously decays and emits a short burst of coherent photons. For higher

Pirmin Tischler and Valerie Y. Horter contributed equally to this work.

excitation densities, the intensity increases quadratically while the temporal width of the peak decreases linearly [4]. Since the dipoles start out incoherent and first need to synchronize, there is a delay time between excitation and emission that becomes shorter for higher dipole densities. The coherent emission leads to a directionality of the photons. At excitations close to the threshold, intensity fluctuations in the transient signals can be observed [5, 6]. The signal exhibits so called Burnham-Chiao ringing [7] whereby dampened oscillations of the macroscopic polarization are characteristic for this emission process. So far, SF in solid state systems has mainly been observed at cryogenic temperatures or high magnetic fields [8–11]. Huang et al. showed SF in lanthanide-doped upconversion nanoparticles (UCNPs) at room temperature [12]. Recently, Biliroglu et al. reported SF at temperatures up to 300 K in phenetylammonium caesium lead bromide (PEA:$CsPbBr_3$) a quasi-2D perovskite [13]. They observed a spectrally narrow feature rising out of the photoluminescence (PL) spectrum at 2.36 eV for excitation above a threshold of 4 μJ cm^{-2} at 80 K and 25 μJ cm^{-2} at 300 K. Moreover, a decrease of the decay time and some oscillations were observed in the transient emission behavior.

Short bursts of photons, however, are not only a characteristic feature of SF but also of amplified spontaneous emission (ASE). Here, photons generated by spontaneous emission propagate through the medium and interact with excited states in the environment. This leads to stimulated emission and a collective amplification. The process relies on a sequence of spontaneous emission, photon propagation, and stimulated emission. Therefore, suppressing waveguiding and thus photon propagation also suppresses ASE [14, 15], while for SF the quantum mechanical coupling of neighboring emitters without the need of photon propagation is crucial. Transient ASE investigations have also shown ringing [16–18] similar to Burnham-Chiao ringing for SF. This behavior can be explained by hot carrier relaxation on the same timescale as the ASE process. ASE also exhibits a time delay between excitation and emission peak due to relaxation processes after photoexcitation and the time it takes for critical gain to be reached via propagation of photons [17, 19].

Additionally, for a mixed material system as discussed here, a resupply of charge carriers from the energetically higher lying 2D material to the 3D bulk material can lead to a slower rising flank of the emission and therefore a delayed peak maximum in the transient signal.

SF has also been used to explain the emission behavior of coupled $CsPbBr_3$ quantum dot superlattices at temperatures of 6 K by Rainò et al. [20]. Here, the emission exhibits a feature at around 2.31 eV with a full-width at half maximum (FWHM) of 11 meV. Qualitatively similar observations as made in [13] are reported. Rainò et al. present a shortening of the decay for higher excitation fluences from about 600 ps at 0.05 μJ cm^{-2} to about 15 ps at 10^3 μJ cm^{-2} as well as Burnham-Chiao ringing for excitation fluences above 60 μJ cm^{-2}.

ASE in the related material system $CsPbBr_3$ has been reported by multiple groups [21–26]. The ASE can be detected after reaching a certain threshold of the excitation fluence, ranging from 26 μJ cm^{-2} to 750 μJ cm^{-2}. The lasers used as excitation source ranged from wavelengths of 337 to 405 nm and from pulse durations of 50 fs to 6 ns. For this material system, the photoluminescence (PL) maximum is found at around 520–530 nm (2.34–2.38 eV) with FWHM of 16–26 nm (90–120meV). For excitation densities surpassing the ASE threshold, an additional narrow ASE peak arises at 530–540 nm (2.34–2.30 eV) with FWHM of about 2–7 nm (10–30 meV).

While ASE and SF lead to similar observations, the physical origin is qualitatively different in the two cases. For ASE, the burst is created from incoherent excited states inside the gain material, gaining its transient and spectral properties from the collective creation of photons during stimulated emission. For SF, the light is emitted from an ensemble of excited states that synchronize through quantum mechanical coupling prior to emission. We show evidence that the spectral narrowing that arises above threshold in the emission spectrum of PEA:$CsPbBr_3$ is not due to SF but can be explained by ASE.

2 | Results and Discussion

In our experiments, we carry out optical measurements on samples prepared following a slightly adjusted recipe published by Biliroglu et al. in [13]. The PEA:$CsPbBr_3$ samples are fabricated on glass substrates (a scheme of the crystal structure of the samples is shown in Figure S1). To confirm the formation of PEA:$CsPbBr_3$ monolayers, we perform absorption measurements using a Perkin Elmer Lambda1050 spectrophotometer. The resulting absorption spectra at both room-temperature (292 K) and cryogenic temperature (80 K) are given in Figure 1. The most prominent feature in the absorption spectra is the peak at around 2.4 eV that is commonly assigned to the excitonic absorption of bulk $CsPbBr_3$ [27]. In addition, we observe a second feature at 2.87 eV. This peak is assigned to the absorption of a $CsPbBr_3$ monolayer sandwiched between PEA molecules [13]. The peak corresponding to monolayer absorption is most visible at cryogenic temperatures and becomes weaker for higher temperatures while remaining at the same energetic position (see Figure S2). However, it still persists at room temperature, as shown by the differential absorption spectrum given in Figure 1b.

In order to reveal the reported narrowing of the PL emission, we perform time-resolved photoluminescence (TRPL) measurements using a streak-camera and fs pulses as excitation at a temperature of 225 K. The spectra as well as the emission transients show a distinct threshold behavior. Above a threshold of 2.5 μJ cm^{-2} an additional feature is observed in the emission spectra at 530 nm (2.34 eV) with a FWHM of around 7 nm (29 meV, see Figure 1c). This spectral feature is accompanied by a picosecond emission burst on top of the emission transient measured for low excitation densities (see Figure 1d). For fluences below threshold, we observe a PL peak at 520 nm (2.38 eV) with a FWHM of 20 nm (90 meV). This intensity dependent behavior is in line with the observations of Biliroglu et al. with threshold fluences of 4 μJ cm^{-2} at 78 K and 25 μJ cm^{-2} at 300 K. Similar to their observation, we find a decrease in width and delay time between excitation and maximum peak height in our transient measurements. We also observe a transient ringing in the emission transient (see Figure S3). In contrast to Biliroglu et al. we find a different scaling of the transient peak height with the excitation fluence. For SF a power law scaling with an

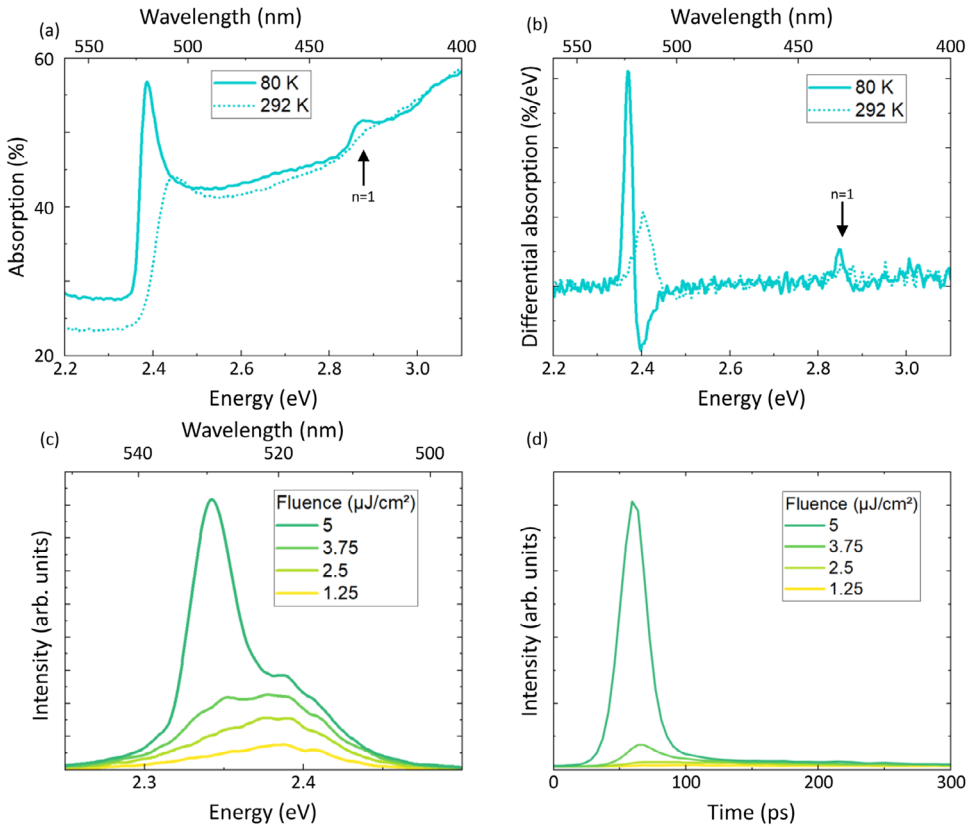

FIGURE 1 | Optical properties of PEA:$CsPbBr_3$ films on a glass substrate. a) Absorption spectra at 80 K (solid line) and 292 K (dashed line), showing the excitonic absorption peaks of the bulk-material at around 2.4 eV and of the monolayer (n = 1) at 2.87 eV. b) First derivative of the absorption, highlighting the n = 1 peak. c) Time-integrated emissions spectra at 225 K for various excitation fluences. A broad spectrum is observed with a narrow feature emerging above a threshold of approximately 2.5 μJ cm^{-2}. d) Transient emission measurements at 225 K and at 531 nm for the same excitation conditions as in c). With higher fluences, a distinct peak evolves and its delay after excitation becomes shorter.

exponent of 2 is expected [5, 28]. However, we find the best power law fit for an exponent of 9.4 for the excitation above threshold. This superlinear growth is not typical for SF. Fitting the same data with an exponential fit improves the fit quality and leads to a scaling of the transient peak height with $e^{2.2F}$ (see Figure S5) which would be expected for ASE [29].

To further clarify whether the emission behavior is dominated by cooperative (i.e., SF) or collective emission (i.e., ASE), we suppressed waveguiding to hamper the collective emission.

ASE and SF can coexist in the same material system [16]. To suppress waveguiding is not expected to suppress SF, since it is a cooperative effect relying on a synchronization of dipoles prior to emission rather than a collective emission mechanism where propagating photons lead to stimulated emission and thus ASE. ASE can be suppressed by suppression of waveguiding [14]. Therefore, since suppression of waveguiding suppresses the propagation of real photons in waveguide modes, it is mainly and strongly affecting ASE.

SF on the other hand relies on the coupling of dipoles via all photonic modes and works also without an underlying waveguide. As the overall photonic mode structure is only slightly modified, the effect of the substrate is expected to be much less relevant. To be more precise, SF is expected to be mainly influenced by the excitation area. However, the maximum area that can contribute to SF is restricted by the coherence time of excited emitters. The latter is not being influenced significantly by the underlying substrate. Therefore, we can fully suppress the proportion of the emission that is caused by ASE and the remaining emission is then due to SF.

For this we fabricated samples with substrates made of Si with a 90 nm layer of SiO_2 as well as bulk SiO_2 as shown in Figure 2. Since the refractive index of silicon is higher than that of the perovskite, there is no critical angle of total internal reflection for the light generated inside the sample, waveguiding is suppressed and photons not directly emitted into the escape cone are absorbed in the silicon substrates. Using this layer sequence suppresses ASE [14, 15], while it is expected to not have any effect on quantum mechanical coupling determining SF. Since silicon has a lower conduction band than the perovskite, an additional layer of isolating SiO_2 is necessary to prevent excited charge carriers from transferring into the silicon. We choose a thickness of 90 nm to guarantee the electrical isolation while the evanescent field transfers photons into the substrate. To rule out surface effects being a dominant contributor to the behavior on the silicon substrate, samples were also created on a bulk SiO_2 quartz substrate. Since SiO_2 has a lower refractive index compared to the perovskite, it serves as a substrate that has both the waveguiding characteristics of the sample on glass substrate

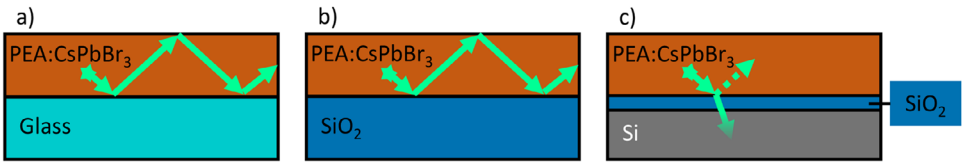

FIGURE 2 | Scheme of the different samples comprising a perovskite layer and different substrates. a) Glass substrate b) SiO_2 substrate. c) Si substrate with 90 nm of SiO_2 on top. a) and b) allow for waveguiding in the perovskite while in c) waveguiding is suppressed.

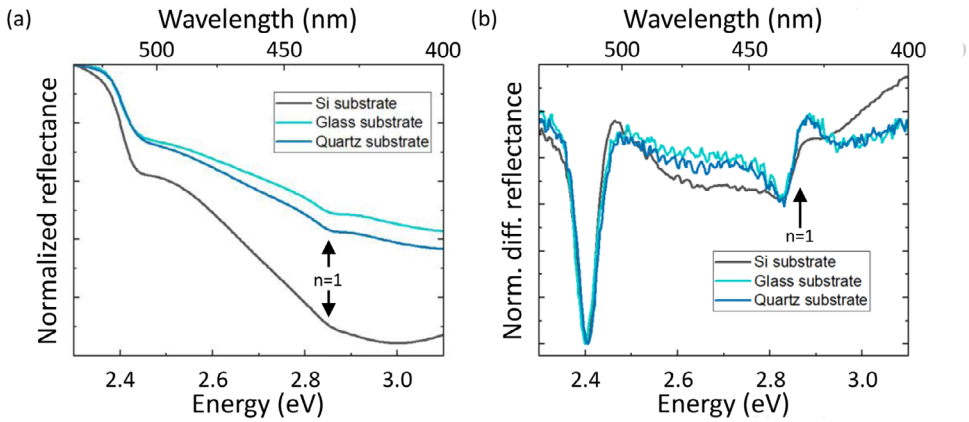

FIGURE 3 | Reflectance measurements for the different substrates. a) Reflectance spectra of the samples on different substrates displaying similar shapes for all substrates with a stronger absorption for the silicon substrate at higher energies also suppressing the reflection. b) First derivative of the reflectance measurement, highlighting the n = 1 layer that sits at the same energetic position for all three substrates.

as well as the same surface on which the sample material is deposited as the silicon substrate.

We verified that the sample preparation on Si and on SiO_2 yields the same perovskite composition as on the glass substrate. Since the Si substrate is opaque, it is not possible to measure transmission and hence absorption. We compared the reflectance for the different substrates as showcased in Figure 3. All reflectance curves display similar shape, including the n = 1 feature at 2.87 eV. This feature becomes more obvious in the differential reflectance.

Additionally, we use a profilometer to determine the thicknesses. The thickness is found to be roughly 80 nm on glass and 90 nm on silicon, respectively. We also check for uniformity and compare the surface roughness with an AFM (Figure S6) which yields a mean surface roughness of about 1 nm for the glass substrate and 7 nm for the silicon substrate. Finally, also XRD was measured (Figure S7). We find comparable crystallinity for the two substrates.

Angle-dependent emission measurements for PEA:$CsPbBr_3$ on the different substrates demonstrate the different waveguiding behavior as showcased in Figure 4. Here, we differentiate surface emission and edge emission. For surface emission the sample is excited at an angle of 45° to the surface normal. For edge emission the sample is excited parallel to the surface normal. In both cases the emission is detected perpendicular to the excitation, i.e., at 45° to the surface normal in case of surface emission and perpendicular to the surface normal for edge emission. For the glass substrate, the PL is significantly more pronounced when the edge emission is measured compared to the forward emission. For the Si substrate the opposite is the case, demonstrating a suppression of waveguiding in the sample. This effect also persists for low temperatures (80 K) as shown in Figure S4.

The intensity dependent emission of the PEA:$CsPbBr_3$ on the different substrates is investigated with a sub-nanosecond pulsed laser as shown in Figure 5. Since the laser used here has a pulse length of 800 ps, the fluence thresholds are higher than in Figure 1. The thresholds in peak power densities of the ps laser and the fs laser are comparable and in the order of tens of MW cm^{-2}. On the glass substrate an additional peak appears at a threshold of about 2.3 mJ cm^{-2} for a temperature of 80 K. For the SiO_2 substrate the threshold is at a comparable value at around 1.9 mJ cm^{-2}. In contrast, for the Si substrate, even for fluences of over 100 mJ cm^{-2} no additional narrow emission feature is observed.

This shows that the suppression of waveguiding inside the PEA:$CsPbBr_3$ leads to a suppression of the spectrally narrow emission feature. We conclude from this that this additional peak can be clearly explained by ASE since this effect strongly depends on the waveguiding properties of the sample. We do not find any evidence for SF.

3 | Conclusion

We have investigated the intensity-dependent emission in PEA:$CsPbBr_3$ deposited on different substrates with different waveguiding behavior. We have demonstrated that the spectrally narrow emission occurs for perovskite film on glass and SiO_2 while it is suppressed on an Si substrate. This has led to the

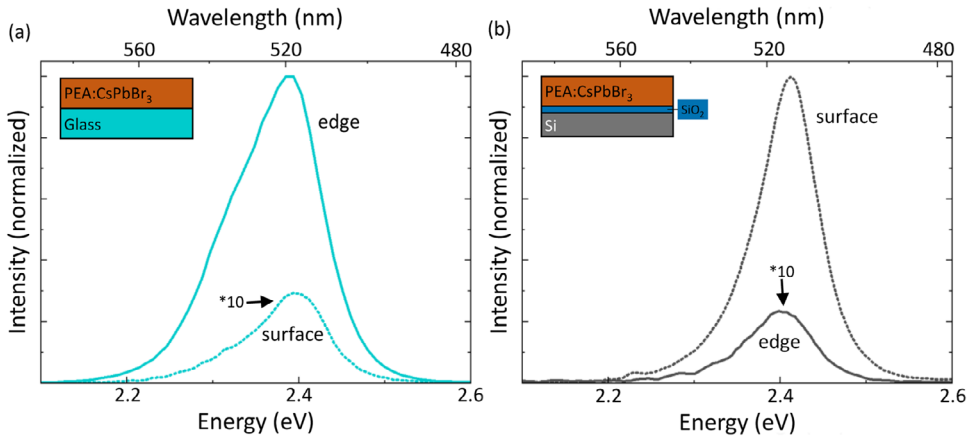

FIGURE 4 | Comparison of edge (solid line) and surface emission (dashed line) for the perovskite layer on glass and on Si substrate, respectively. a) For the glass substrate the emission is higher for edge emission. b) For the Si substrate the emission is higher when detected from the surface.

conclusion that ASE rather than SF is the underlying mechanism. Our results contrast with the recently published notion [13] of SF being the relevant mechanism for the high excitation emission in PEA:$CsPbBr_3$.

4 | Methods

4.1 | Sample Synthesis

The glass substrates used are microscope slides from Epredia containing SiO_2 (69-74 %), Na_2O (10-16 %), CaO (5-14 %), MgO (0%–6%) and Al_2O_3 (0%–3%).

For the synthesis of the samples first the substrates are cut into 16×16 mm^2 and cleaned in an ultrasonic bath with first water then acetone and then isopropanol before being plasma treated. Solutions are prepared of $PEABr_3$ in DMSO (2.8 M, 565.9 mg ml^{-1}) and 18-Crown-6 in DMSO (300 mg ml^{-1}). 231.9 mg $CsPbBr_3$ with 1 mL DMSO are mixed with 57 µl of the first solution and 17.9 µl of the second solution. This final solution is placed on a hot plate at 60°C for 10–15 min. 50 µl of this solution are spin coated on the substrates with 1000 RPM for 20 s with an acceleration of 1000 RPM s^{-1} and then 4000 RPM for 40 s with an acceleration of 1000 RPM s^{-1}. The samples then are annealed at 70°C for 10 min.

Solutions are prepared of $PEABr_3$ in DMSO (2.8 M, 565.9 mg ml^{-1}) and 18-Crown-6 in DMSO (300 mg ml^{-1}). $CsPbBr_3$ (231.9 mg) with DMSO (1 mL) are mixed with 57 µl of the first solution and 17.9 µl of the second solution. This final solution is placed on a hot plate at 60°C for 10–15 min. 50 µl of this solution are spin coated on the substrates with 1000 RPM for 20 s with an acceleration of 1000 RPM s^{-1} and then 4000 RPM for 40 s with an acceleration of 1000 RPM s^{-1}. The samples then are annealed 70°C for 10 min.

4.2 | Absorption and Reflection

Absorption and reflection measurements were performed with a Lambda1050 UV/Vis spectrophotometer.

4.3 | Streak Camera Measurements

Transient photoluminescence was measured using a Universal Streak Camera (Hamamatsu C10901) equipped with a S20 photo cathode. For spectral dispersion a Kymera 328i Spectrograph was used. The sample was excited with a Light Conversion Pharos 100 femtosecond laser using ORPHEUS optical parametric amplifiers from light conversion. If not otherwise specified a wavelength of 434 nm and a pulse frequency of 2 kHz was used. The sample was mounted and cooled via an OptistatDry TLEX closed cycle helium cryostat.

4.4 | Surface and Edge Emission of Photoluminescence

Time-integrated, angle-dependent photoluminescence was measured using an FLS920 Fluorescence Spectrometer from Edinburgh Instruments with excitation at 355 nm selected from the spectrum of a xenon lamp.

4.5 | Photoluminescence with Pulsed Laser

Time integrated photoluminescence was measured with an Acton SpectraPro SP-2300 spectrometer and a Pi-Max 4 camera. For excitation an Innolas piccolo-10 pulsed laser was used with a wavelength of 355 nm and a pulse frequency of 10 kHz. The sample was mounted inside a home-build cryostat using a cold finger that is cooled by liquid nitrogen.

4.6 | Atomic Force Microscopy

Atomic Force Microscopy (AFM) was measured using a NanoWizard II from JPK.

4.7 | Profilometer

Measurements of the surface profile and the thickness were performed using a Dektak XT from Bruker Instruments. The

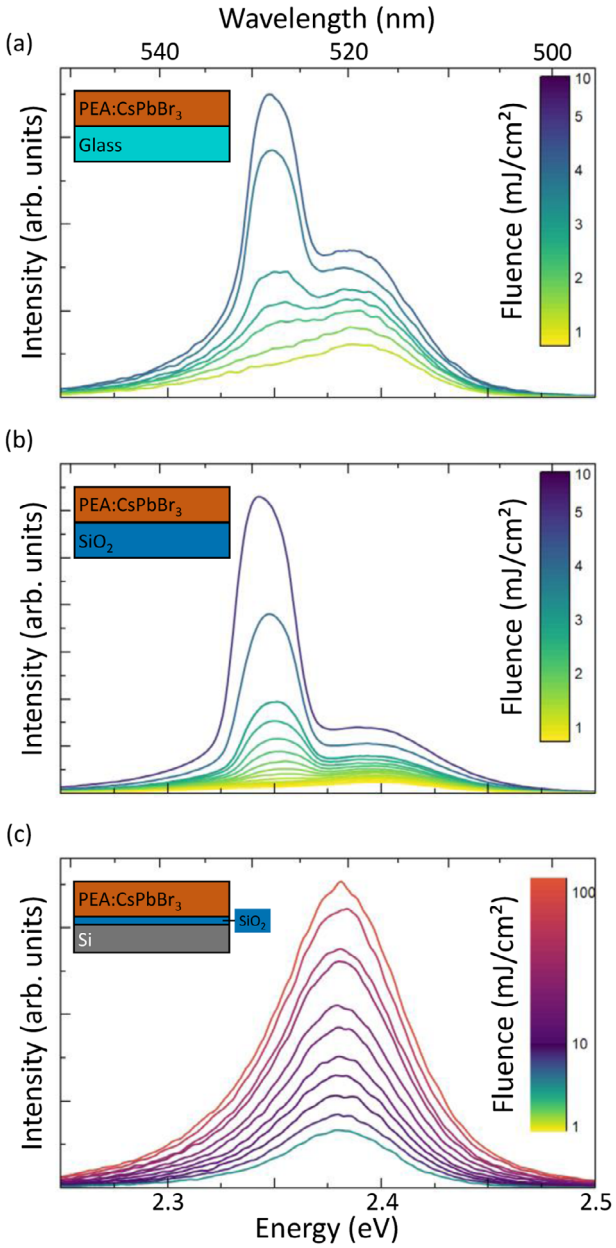

FIGURE 5 | Comparison of threshold behavior for all substrates at 80 K. Samples on (a) the glass substrate and (b) the SiO_2 substrate show an additional narrow emission peak when the excitation surpasses a threshold of around 2 mJ cm^{-2}. (c) The sample on the Si substrate does not exhibit this additional peak even for high fluences above 100 mJ cm^{-2}.

probing force was set to 2 mg. To determine the thickness of the sample, a thin line was scratched with a steel needle. The thickness was determined by using the step function of the software which averages the valley found in the measurement as a reference.

4.8 | XRD

X-ray diffraction was measured using Cu $K\alpha_1$ and $K\alpha_2$ radiation with a Bruker D2 Phaser Diffractometer with a Lynxeye Xe-T detector.

Acknowledgements

The project was funded by the Deutsche Forschungsgemeinschaft (DFG, German Research Foundation) via project PEROLAS (funding code: 409035484) and under Germany's Excellence Strategy via the Excellence Cluster "3D Matter Made to Order" (EXC-2082/2-390761711), the Karlsruhe School of Optics & Photonics (KSOP), the National Natural Science Foundation of China (no. 62404143), and the Natural Science Foundation Project of Sichuan Province (no. 2025ZNSFSC1423).

Funding

The project was funded by the Deutsche Forschungsgemeinschaft (DFG, German Research Foundation) via project PEROLAS (funding code: 409035484) and under Germany's Excellence Strategy via the Excellence Cluster "3D Matter Made to Order" (EXC-2082/2-390761711), the Karlsruhe School of Optics & Photonics (KSOP), the National Natural Science Foundation of China (no. 62404143), and the Natural Science Foundation Project of Sichuan Province (no. 2025ZNSFSC1423).

Conflicts of Interest

The authors declare no conflicts of interest.

Data Availability Statement

The data that support the findings of this study are available from the corresponding author upon reasonable request.

References

1. O. Hess, "Nanoplasmonic cavity quantum electrodynamic architectures for room-temperature quantum technologies," *The European Physical Journal Special Topics* 235 (2025): 2875–2885, https://doi.org/10.1140/epjs/s11734-025-02066-0.

2. R. Y. Teh, L. Rosales-Zarate, P. D. Drummond, and M. D. Reid, "Mesoscopic and macroscopic quantum correlations in photonic, atomic and optomechanical systems," *Progress in Quantum Electronics* 90 (2023): 100396, https://doi.org/10.1016/j.pquantelec.2022.100396.

3. T. Farrow and V. Vedral, "Classification of macroscopic quantum effects," *Optics Communications* 337 (2015): 22–26, https://doi.org/10.1016/j.optcom.2014.06.042.

4. M. S. Malcuit, J. J. Maki, D. J. Simkin, and R. W. Boyd, "Transition From Superfluorescence to Amplified Spontaneous Emission," *Physical Review Letters* 59, no. 11 (1987): 1189–1192, https://doi.org/10.1103/PhysRevLett.59.1189.

5. M. Gross and S. Haroche, "Superradiance: An essay on the theory of collective spontaneous emission," *Physics Reports* 93, no. 5 (1982): 301–396, https://doi.org/10.1016/0370-1573(82)90102-8.

6. J. J. Maki, M. S. Malcuit, M. G. Raymer, and R. W. Boyd, "Influence of collisional dephasing processes on superfluorescence," *Physical Review A* 40, no. 9 (1989): 5135–5142, https://doi.org/10.1103/PhysRevA.40.5135.

7. D. C. Burnham and R. Y. Chiao, "Coherent Resonance Fluorescence Excited by Short Light Pulses," *Physical Review* 188, no. 2 (1969): 667–675, https://doi.org/10.1103/PhysRev.188.667.

8. D. C. Dai and A. P. Monkman, "Observation of superfluorescence From a quantum ensemble of coherent excitons in a ZnTe crystal: Evidence for spontaneous Bose-Einstein condensation of excitons," *Physical Review B* 84, no. 11 (2011): 115206, https://doi.org/10.1103/PhysRevB.84.115206.

9. G. Timothy Noe II, J.-H. Kim, J. Lee, et al., "Giant superfluorescent bursts From a semiconductor magneto-plasma," *Nature Physics* 8 (2012): 219–224, https://doi.org/10.1038/nphys2207.

10. R. Florian, L. O. Schwan, and D. Schmid, "Two-color superfluorescence of O2- centers in KCl," *Journal of Luminescence* 31-32 (1984): 169–171, https://doi.org/10.1016/0022-2313(84)90237-0.

11. K. Miyajima, Y. Kagotani, S. Saito, M. Ashida, and T. Itoh, "Superfluorescent pulsed emission From biexcitons in an ensemble of semiconductor quantum dots," *Journal of Physics: Condensed Matter* 21 (2009): 195802, https://doi.org/10.1088/0953-8984/21/19/195802.

12. K. Huang, K. K. Green, L. Huang, H. Hallen, G. Han, and S. F. Lim, "Room-temperature upconverted superfluorescence," *Nature Photonics* 16 (2022): 737–742, https://doi.org/10.1038/s41566-022-01060-5.

13. M. Biliroglu, G. Findik, J. Mendes, et al., "Room-temperature superfluorescence in hybrid perovskites and its origins," *Nature Photonics* 16, no. 16 (2022): 324–329, https://doi.org/10.1038/s41566-022-00974-4.

14. I. Allegro, Y. Li, B. S. Richards, U. W. Paetzold, U. Lemmer, and I. A. Howard, "Bimolecular and Auger Recombination in Phase-Stable Perovskite Thin Films From Cryogenic to Room Temperature and Their Effect on the Amplified Spontaneous Emission Threshold," *The Journal of Physical Chemistry Letters* 12, no. 9 (2021): 2293–2298, https://doi.org/10.1021/acs.jpclett.1c00099.

15. A. Haugeneder, M. Neges, C. Kallinger, et al., "Nonlinear emission and recombination in conjugated polymer waveguides," *Journal of Applied Physics* 85, no. 2 (1999): 1124–1130, https://doi.org/10.1063/1.369237.

16. E. Kobiyama, G. Rainò, Y. Berezovska, et al., "Transition Between cooperative emission regimes in giant perovskite nanocrystals," *Nature Materials* 25 (2026): 1146–1153, https://doi.org/10.1038/s41563-026-02544-3.

17. A. P. Schlaus, M. S. Spencer, K. Miyata, et al., "How lasing happens in $CsPbBr_3$ perovskite nanowires," *Nature Communications* 10, no. 1 (2019): 265, https://doi.org/10.1038/s41467-018-07972-7.

18. C. Kallinger, S. Riechel, O. Holderer, U. Lemmer, and J. Feldmann, "Picosecond amplified spontaneous emission bursts From a molecularly doped organic semiconductor," *Journal of Applied Physics* 91, no. 10 (2002): 6367–6370, https://doi.org/10.1063/1.1466879.

19. M. Li, J. Fu, Q. Xu, and T. C. Sum, "Slow Hot-Carrier Cooling in Halide Perovskites: Prospects for Hot-Carrier Solar Cells," *Advanced Materials* 31, no. 47 (2019): 1802486, https://doi.org/10.1002/adma.201802486.

20. G. Rainò, M. A. Becker, M. I. Bodnarchuk, R. F. Mahrt, M. V. Kovalenko, and T. Stöferle, "Superfluorescence From lead halide perovskite quantum dot superlattices," *Nature* 563, no. 7733 (2018): 671–675, https://doi.org/10.1038/s41586-018-0683-0.

21. Y. Li, H. Hu, A. Farag, et al., "Enhancement of Amplified Spontaneous Emission by Electric Field in $CsPbBr_3$ Perovskites," *Nano Letters* 23, no. 5 (2023): 1637–1644, https://doi.org/10.1021/acs.nanolett.2c02944.

22. M. L. De Giorgi, F. Krieg, M. V. Kovalenko, and M. Anni, "Amplified Spontaneous Emission Threshold Reduction and Operational Stability Improvement in CsPbBr3 Nanocrystals Films by Hydrophobic Functionalization of the Substrate," *Scientific Reports* 9 (2019): 17964, https://doi.org/10.1038/s41598-019-54412-7.

23. X. Tian, R. Wei, Z. Ma, and J. Qiu, "Amplified Spontaneous Emission From Perovskite Quantum Dots Inside a Transparent Glass," *Advanced Optical Materials* 10, no. 6 (2022): 2102483, https://doi.org/10.1002/adom.202102483.

24. D. A. Tatarinov, S. S. Anoshkin, I. A. Tsibizov, et al., "High-Quality CsPbBr 3 Perovskite Films With Modal Gain Above 10 000 cm −1 at Room Temperature," *Advanced Optical Materials* 11, no. 7 (2023): 2202407, https://doi.org/10.1002/adom.202202407.

25. S. Milanese, M. L. De Giorgi, M. Anni, M. I. Bodnarchuk, and L. Cerdán, "Rationalizing the Amplified Spontaneous Emission Mechanism in $CsPbBr_3$ Perovskite Nanocrystals Films by means of Optical Gain Measurements," *Advanced Optical Materials* 12, no. 27 (2024): 2401078, https://doi.org/10.1002/adom.202401078.

26. N. Enea, F. Tommasi, L. Forcieri, et al., "Room temperature amplified spontaneous emission in CsPbBr3 polycrystalline thin films in transmission configuration," *AIP Advances* 15, no. 2 (2025): 025219, https://doi.org/10.1063/5.0246259.

27. T. R. Hopper, A. Jeong, A. Gorodetsky, et al., "Kinetic modelling of intraband carrier relaxation in bulk and nanocrystalline lead-halide perovskites," *Physical Chemistry Chemical Physics* 22, no. 31 (2020): 17605–17611, https://doi.org/10.1039/d0cp01599g.

28. K. Cong, Q. Zhang, Y. Wang, G. T. Noe, A. Belyanin, and J. Kono, "Dicke superradiance in solids [Invited]," *Journal of the Optical Society of America B* 33, no. 7 (2016): C80–C101, https://doi.org/10.1364/JOSAB.33.000C80.

29. A. E. Siegman "*Lasers*," Oxford University Press (1986), ISBN: 978–0935702118.

Supporting Information

Additional supporting information can be found online in the Supporting Information section.

Supporting file: adom71710-sup-0001-SuppMat.docx.